Title

Local electronic structure of histidine in aqueous solution

Journal

Physical Chemistry Chemical Physics, 23(14)

ISSN

0956-5000

Authors

Kostko, O

Xu, B

Ahmed, M

Publication Date

2021-04-14

DOI

10.1039/d1cp00361e

Peer reviewed

Local electronic structure of histidine in aqueous solution

O. Kostko,[1,2,a)] B. Xu,[1] and M. Ahmed[1]

[1] Chemical Sciences Division, Lawrence Berkeley National Laboratory, Berkeley, CA 94720, USA

2 Advanced Light Source, Lawrence Berkeley National Laboratory, Berkeley, CA 94720, USA

a) Electronic mail: OKostko@lbl.gov

ABSTRACT

The local electronic structure of aqueous histidine, an amino acid important in nature and biology, is revealed by aerosol X-ray photoemission spectroscopy. A detailed picture of the photoionization dynamics emerges by tuning the pH of the aqueous solution from which the aerosols are generated allowing us to report the X-ray photoelectron spectroscopy (XPS) of histidine. Assignment of the experimental photoelectron spectra of the C1s and N1s levels allows for determination of the protonation state of histidine in these aqueous aerosols and is confirmed by density functional calculations. XPS spectra show that at pH = 1, both imidazole and amine group nitrogens are protonated, at pH = 7, the amine group nitrogen is protonated and carboxyl group carbon is deprotonated resulting in zwitterionic structure and at pH = 13, only the carboxyl group remains deprotonated. Comparison of these results with previous experimental and theoretical results suggests that X-ray spectroscopy on aqueous aerosols can provide a convenient and simple way of probing electronic structure in aqueous solutions.

INTRODUCTION

Amino acids constitute the elementary building blocks of proteins, are metabolic intermediates, and play important roles in living organisms. To advance our understanding of their roles and functions in biology, it is important to determine the electronic and geometric structure of amino acids particularly in a solvent environment such as water. X-ray spectroscopic techniques are powerful tools for investigations of electronic structure of matter and have been extensively applied to amino acids. However, most of these investigations have been restricted to solid state[1–8] or the gas phase amino acids[9–12] while biochemical systems almost universally occur in aqueous environment. In the gas phase, amino acids exclusively exist in the neutral (molecular) form,[13–15] and they are zwitterionic in the condensed phase.[16] In biologically relevant aqueous environments, amino acids exist in a wide variety of charge states whose relative populations are determined by the pH of the solution. Amino acids exist as a cation in acidic media with its amine group protonated, whereas the carboxyl group is neutral. For a basic solution, the amine and carboxyl groups are both deprotonated and the amino acid acts as an anion. For intermediate pH values, amino acids form a zwitterionic state, leading to an overall charge-neutral state.

Histidine is an amino acid with an imidazole ring side chain, the charge state of which depends on the environmental pH (Fig. 1).[17–19] Because of its pH-dependent protonation, histidine is involved in the functions of proteins[20] and plays a very important role in proton conduction,[21] enzyme catalysis,[22] and metal-requiring enzymes.[23] From the viewpoint of molecular assembly in synthetic biology, amino acids and peptides can play very important roles due to their side chains,[24,25] and in the case of histidine, the possibility of the imidazole motif to π-stack and act as nucleation sites. Recently, we demonstrated a self-assembly process in arginine-oleic acid solutions, which is pH dependent leading to the formation of micelles, vesicles and finally sponges in basic medium.[26] In histidine derived peptides, liquid-liquid phase separations have been invoked to give rise to the formation of hydrogels or coacervate micro-droplets which are also pH dependent.[27] The imidazole motif prevalent in histidine has also been implicated in nucleation and crystallization processes in concentrated aqueous media, however neutron diffraction and X-ray scattering studies suggest that it is solvation which drives assembly and not π-stacking of the imidazole pairs.[28]

Several X-ray absorption,[29,30] X-ray emission,[31] and resonant inelastic X-ray scattering (RIXS)[32,33] studies have been conducted on glycine, proline, cysteine, and lysine to investigate the change of their electronic structures engendered by varying the pH of solutions. The above mentioned techniques provide a view of the bulk solution, while X-ray photoelectron spectroscopy (XPS), which can provide direct information on electronic structure of the surface and interface, brings an extra layer of sensitivity to the measurements. However only recently has it been applied for the study of highly volatile aqueous solutions via liquid jet[34] technology, to probe the electronic structure of lysine,[35] glycine,[36] and imidazole[37] (the side chain of histidine), while we have pioneered the use of aqueous aerosols to investigate arginine with XPS[38] and valence band spectroscopy.[39] The XPS studies revealed large spectral energy shifts of the N1s and C1s photoemission peaks as a function of pH, showing it has a large influence on the electronic structure of amino acids.

While the solution phase pH dependence has been probed by vibrational spectroscopy[40] and NMR methods,[17] most of X-ray studies to date have focused on solid state histidine. XPS[8,41,42] and near-edge X-ray absorption fine structure (NEXAFS)[2,43] measurements of solid histidine and other biomolecules were supported by theoretical investigation of NEXAFS spectra of amino acids.[44] A recent publication discusses NEXAFS and RIXS of histidine's N K-edge in aqueous solution at basic, neutral, and acidic conditions.[45] In the present work, we report on the impact of the pH variation on the local electronic structure of histidine in solution using XPS applied to the aqueous aerosols combined with theory. We demonstrate that we can extract protonation states of both carbon and nitrogen atoms at various pH conditions revealing valuable information for small biomolecules.

METHODS

Histidine was obtained commercially from Sigma-Aldrich (purity above 99%) and used without further purification. Initial 0.1 mol/L amino acid solutions were prepared with highly demineralized water. pH values of 1.0, 7.0, and 13.0 (±0.2) were adjusted either with hydrochloric acid or sodium hydroxide.

In this study, a velocity map imaging (VMI) spectrometer combined with an aerodynamic lens[38,46] was used to obtain the XPS of histidine aqueous aerosol nanoparticles. Aqueous aerosol nanoparticles were generated by atomizing 0.1 mol/L histidine aqueous solution via a high flux atomizer (Model 3076, TSI). Dry nitrogen is used as carrier gas for the C1s level while oxygen is used for the N1s level measurements. The size distribution of the nanoparticles is measured with a commercial scanning mobility particle sizer (SMPS, TSI). This distribution is broad with a mean particle diameter of 170 nm (surface to volume ratio of 3.7%), providing a nanoscaled solution environment. After passing through a set of aerodynamic lenses, the nanoparticles are tightly focused to a beam. The beam diameter is 1 mm with a computed flux of 10^7 particles/s at the interaction region. The photon beam generated by the beamline 11.0.2 at the Advanced Light Source, Lawrence Berkeley National Laboratory intersects the nanoparticle beam orthogonally and leads to photoemission.

Typical accumulation times for a photoelectron image is about 15 minutes. A background image is collected with an inline filter inserted, which removes all of the nanoparticles from the beam and is subtracted from the data image. The velocity distributions from the background-subtracted reconstructed images is performed using the pBASEX algorithm.[47] The spectrometer is calibrated with N1s spectra of N_2, in order to relate radial position in the image to electron kinetic energy (KE). C1s and N1s spectra presented in the paper are obtained by subtracting a linear background from raw data. The photon energy was calibrated by measuring XPS of nitrogen gas at 425 eV, and the obtained binding energy of N1s is 409.9 eV. Electron binding energies (BE) reported here are with respect to vacuum. Throughout this paper, when molecular formula fragments are reported, the atom of interest is indicated by being underlined where there is possible ambiguity.

Theoretical photoelectron spectra are calculated using the Gaussian 09 computational chemistry package to help assignment of experimental XPS data.[48] Geometrical structures of histidine molecules are optimized using ωB97X-D functional with a 6-311+g(d,p) basis set in the presence of solvent simulated by the polarizable continuum model (PCM). The XPS peak positions and corresponding chemical shifts are obtained using Koopmans' theorem (also known as "initial state") approximation for

the density functional theory.[49] According to the approximation, the final state effects are neglected and electron BEs and corresponding BE shifts are found only for initial state of the molecule. While the method is not very accurate for finding absolute values of BEs, it is rather precise and widely used to predict BE shifts. Calculated values of binding energies are blue shifted by 9.3 eV for C1s and by 10.9 eV for N1s electrons to correlate with experimental data for histidine solution with pH = 7.

RESULTS AND DISCUSSION

Photoelectron spectra of aqueous solutions of histidine at three different pH values are shown in Fig. 2. XPS spectra of the N1s level are collected using the photon energy of 425 eV, whereas the C1s spectra are collected at photon energy of 310 eV, resulting in kinetic energy of emitted electrons of 20 eV. While the shape of C1s spectra at three different pH values are very similar, the N1s spectrum becomes broader with the increase of pH, but the common trend is that both N1s and C1s peaks shift to lower binding energy with the increase of pH. That is due to change of the net histidine charge from +2 (cation) at pH = 1, to neutral (the zwitterion form) in neutral solution, to -1 (anion) at pH = 13. The increase of electron density around histidine results in the shift of N1s and C1s peaks to lower BE during the increase of pH.

The experimental spectra were fit using Gaussian functions with fixed FWHM of 1.5 eV in such a way, that the sum of peak areas reflects expected stoichiometric ratios for the chemical environments within the histidine molecule (Fig. 1) and are presented in Table 1. A building block approach, based on literature data on XPS of aqueous solutions of glycine,[36,38] arginine,[38] and imidazole[37] was used to assign the collected experimental data.

At pH = 1, the peak with the highest binding energy of 406.6 eV could be assigned as the amine group (NH_3^+) nitrogen (Fig. 2, left panel). The two remaining peaks are due to the imidazole group. Due to protonation of the imidazole group, both N atoms in the group are in a close chemical environment and therefore corresponding N1s peaks lie near each other at binding energies of 406.0 and 405.6 eV. When the pH of the solution is increased to 7, the imidazole group becomes neutral while the amine group remains protonated. Because all three N atoms are in different environments, the three peaks used to fit the experimental data are well separated. The peak corresponding to the unchanged amine group, shifts to slightly lower binding energy of 406.1 eV. Whereas both imidazole N atoms experience stronger BE shifts: the N=C–NH and N=C–NH 1s photoemission lines occur at 405.0 and 403.6 eV, respectively. At pH = 13, both the amine and imidazole groups are deprotonated. The imidazole group maintains the same charge as at pH = 7 and therefore N=C–NH peak stays at 405.0 eV, whereas N=C–NH peak shifts to lower BE of 403.2 eV, separating the imidazole group peaks by 1.8 eV, what is close to the experimental value of 1.7 eV reported for aqueous imidazole.[37] In agreement with previous XPS studies of aqueous glycine,[36,38] deprotonation of the amine group leads to a significant decrease of corresponding N1s BE by 2.0 - 2.5 eV and results in amine's N1s peak of histidine at 403.9 eV.

The shape of C1s spectra (Fig. 2, right panel) does not change so strongly as that of the N1s spectra. All three spectra have a shoulder at high BE which is due to the ionization of the carboxyl group and correlates well with the similar peak in glycine.[36,38] The larger peak in C1s spectra is due to photoemission from the remaining five carbon atoms, which complicates assignment of the individual peaks. The lowest BE component could be due to aliphatic C–C carbon, whereas the two peaks in

between of carboxyl and aliphatic carbons should be due to imidazole's and amine's C1s peaks. According to previous XPS data for imidazole[37] and glycine,[36,38] at pH =1 the peak at 291.6 eV is due to the amine group and N=C–NH carbon in the imidazole group. Two remaining imidazole carbons (labeled C–N in Fig. 2) result in a peak at 290.9 eV. Increase of pH to 7 leads to deprotonation of the carboxyl group, which shifts the corresponding peak BE by 0.8 eV, what is less than that observed in glycine (1.0 eV[36] or 1.1 eV[38]), but larger than that observed in arginine (0.7 eV[38]). Deprotonation of the imidazole group and change of net molecule's charge from +2 to 0 leads to decrease of BE of the remaining peaks, but does not change their order. The peak at 290.8 eV is due to glycine's and imidazole's N=C–NH carbons, whereas the peak at 290.0 eV is due to two other imidazole's carbon atoms. Increase of pH to 13 leads to deprotonation of the amine group and change of peak order within the large peak in histidine's C1s XPS spectrum (Fig. 2, bottom right panel). The imidazole's N=C–NH carbon appears at BE = 290.5 eV, whereas the amine's carbon ($C–NH_2$) shifts to BE of 290.0 eV, joining two imidazole's carbons.

While the building block's approach allows for a tentative assignment of the XPS spectra, we performed theoretical calculation as outlined above to confirm these assignments and gain further insight into the electronic structure of solvated histidine. To reproduce the experimental spectra, in particular the splitting on carboxyl's carbon it was necessary to explicitly insert four water molecules around histidine molecule as shown in Fig. S1 in Supporting Information. This model at various levels of theory have been implemented in studying the core level shifts in aqueous glycine.[36,50,51] The calculated spectra, based on binding energies summarized in Table 2, are convoluted with a Gaussian with FWHM = 1.2 eV to resemble experimental spectra and are shown in Fig. 3. The calculated spectra reproduce the main features of the experimental XPS spectra. Thus for the N1s peak, one can see that the peak gets broader at pH = 7 and pH = 13, and the asymmetric shape of the peaks at those pH is well reproduced. The theory confirms our assignment with only one major difference: deprotonation of the amine group caused by increase of pH from 7 to 13 leads to decrease of corresponding N1s BE by 3.1 eV instead of the 2.2 eV observed in the experiment, shifting the primary amine's nitrogen from the most bound at pH = 1 and 7 to the least bound at pH = 13. The observed discrepancy with the experiment may arise from the simple level of theory to extract electron BE's, namely Koopmans' theorem. However, the correlation of theory with the experiment is better for C1s spectra, reproducing the predicted assignments and shifts of peaks, such as merged Gaussian peaks of double (at pH =1 and 7) or triple (at pH = 13) intensity. In the future, better theoretical models coupled to a higher level of calculations should provide for a more robust fit to our experimental results.

Although we discuss only the π-tautomer of histidine, shown in Figure 1, there is another, τ-tautomer, which has another deprotonated nitrogen in the imidazole moiety.[17–19] Our DFT calculation revealed that the π-tautomer is energetically favorable over the τ-tautomer by 52 meV at pH = 7 and by 25 meV at pH = 13. The computed XPS spectra for both tautomers are presented in Fig. S2 and demonstrate similarity, with one noticeable difference for N1s at pH = 7, where the peak is broader for the τ-tautomer. While the resolution of our experimental spectra does not allow for an unequivocal identification, previous investigations[45] and energetics would suggest that the π-tautomer is the dominant species.

CONCLUSIONS

X-ray photoelectron spectra of histidine aqueous aerosols at different pH values were obtained using the velocity map imaging photoelectron spectrometer combined with an aerodynamic lens. Application of a building block approach allowed for identification of the individual nitrogen and carbon atoms of aqueous histidine by their respective core-level binding energies. Electron binding energies, extracted from DFT calculations of the histidine at different pH values of solution confirmed assignment of the experimental spectra. This allowed for identification of protonation states of individual carbon and nitrogen atoms in histidine molecule. This study also demonstrates that velocity map imaging XPS of aqueous aerosols is a powerful technique allowing to probe the electronic structures of biological molecules in their natural aqueous environment.

CONFLICTS OF INTEREST

There are no conflicts to declare.

ACKNOWLEDGEMENTS

The authors thank Michael Jacobs for help during setup of the experiment. This work is supported by the Condensed Phase and Interfacial Molecular Science Program, in the Chemical Sciences Geosciences and Biosciences Division of the Office of Basic Energy Sciences of the U.S. Department of Energy under Contract No. DE-AC02-05CH11231. This research used resources of the Advanced Light Source, which is a DOE Office of Science User Facility under Contract No. DE-AC02-05CH11231.

REFERENCES

1 M. Schmidt and S. G. Steinemann, XPS studies of amino acids adsorbed on titanium dioxide surfaces, *Fresenius J. Anal. Chem.*, 1991, **341**, 412–415.

2 J. Boese, A. Osanna, C. Jacobsen and J. Kirz, Carbon edge XANES spectroscopy of amino acids and peptides, *J. Electron Spectrosc. Relat. Phenom.*, 1997, **85**, 9–15.

3 J. Hasselström, O. Karis, M. Nyberg, L. G. M. Pettersson, M. Weinelt, N. Wassdahl and A. Nilsson, The Bonding and Electronic Structure Changes upon Adsorption of Important Functional Groups: Glycine on Copper, *J. Phys. Chem. B*, 2000, **104**, 11480–11483.

4 M. Tanaka, K. Nakagawa, T. Koketsu, A. Agui and A. Yokoya, Oxygen K-edge X-ray absorption near edge structures (XANES) of sublimated films of amino acids, *J. Synchrotron Radiat.*, 2001, **8**, 1009–1011.

5 K. Kaznacheyev, A. Osanna, C. Jacobsen, O. Plashkevych, O. Vahtras, Ågren, V. Carravetta and A. P. Hitchcock, Innershell Absorption Spectroscopy of Amino Acids, *J. Phys. Chem. A*, 2002, **106**, 3153–3168.

6 Y. Zubavichus, A. Shaporenko, M. Grunze and M. Zharnikov, NEXAFS Spectroscopy of Homopolypeptides at All Relevant Absorption Edges: Polyisoleucine, Polytyrosine, and Polyhistidine, *J. Phys. Chem. B*, 2007, **111**, 9803–9807.

7 C. P. Schwartz, R. J. Saykally and D. Prendergast, An analysis of the NEXAFS spectra of a molecular crystal: α-glycine, *J. Chem. Phys.*, 2010, **133**, 044507.

8 J. S. Stevens, A. C. de Luca, M. Pelendritis, G. Terenghi, S. Downes and S. L. M. Schroeder, Quantitative analysis of complex amino acids and RGD peptides by X-ray photoelectron spectroscopy (XPS), *Surf. Interface Anal.*, 2013, **45**, 1238–1246.

9 A. R. Slaughter and M. S. Banna, Core-photoelectron binding energies of gaseous glycine: correlation with its proton affinity and gas-phase acidity, *J. Phys. Chem.*, 1988, **92**, 2165–2167.

10 I. Powis, E. E. Rennie, U. Hergenhahn, O. Kugeler and R. Bussy-Socrate, Investigation of the Gas-Phase Amino Acid Alanine by Synchrotron Radiation Photoelectron Spectroscopy, *J. Phys. Chem. A*, 2003, **107**, 25–34.

11 O. Plekan, V. Feyer, R. Richter, M. Coreno, M. de Simone, K. C. Prince and V. Carravetta, Investigation of the Amino Acids Glycine, Proline, and Methionine by Photoemission Spectroscopy, *J. Phys. Chem. A*, 2007, **111**, 10998–11005.

12 O. Plekan, V. Feyer, R. Richter, M. Coreno, M. de Simone, K. C. Prince and V. Carravetta, An X-ray absorption study of glycine, methionine and proline, *J. Electron Spectrosc. Relat. Phenom.*, 2007, **155**, 47–53.

13 W. D. Price, R. A. Jockusch and E. R. Williams, Is Arginine a Zwitterion in the Gas Phase?, *J. Am. Chem. Soc.*, 1997, **119**, 11988–11989.

14 J. Rak, P. Skurski, J. Simons and M. Gutowski, Low-Energy Tautomers and Conformers of Neutral and Protonated Arginine, *J. Am. Chem. Soc.*, 2001, **123**, 11695–11707.

15 M. Remko and B. M. Rode, Effect of Metal Ions (Li+, Na+, K+, Mg2+, Ca2+, Ni2+, Cu2+, and Zn2+) and Water Coordination on the Structure of Glycine and Zwitterionic Glycine, *J. Phys. Chem. A*, 2006, **110**, 1960–1967.

16 P.-G. Jönsson and Å. Kvick, Precision neutron diffraction structure determination of protein and nucleic acid components. III. The crystal and molecular structure of the amino acid α-glycine, *Acta Crystallogr. Sect. B*, 1972, **28**, 1827–1833.

17 S. Li and M. Hong, Protonation, Tautomerization, and Rotameric Structure of Histidine: A Comprehensive Study by Magic-Angle-Spinning Solid-State NMR, *J. Am. Chem. Soc.*, 2011, **133**, 1534–1544.

18 M. Munowitz, W. W. Bachovchin, J. Herzfeld, C. M. Dobson and R. G. Griffin, Acid-base and tautomeric equilibriums in the solid state: nitrogen-15 NMR spectroscopy of histidine and imidazole, *J. Am. Chem. Soc.*, 1982, **104**, 1192–1196.
19 B. Henry, P. Tekely and J.-J. Delpuech, pH and pK Determinations by High-Resolution Solid-State 13C NMR: Acid−Base and Tautomeric Equilibria of Lyophilized l-Histidine, *J. Am. Chem. Soc.*, 2002, **124**, 2025–2034.
20 S. P. Edgcomb and K. P. Murphy, Variability in the pKa of histidine side-chains correlates with burial within proteins, *Proteins Struct. Funct. Bioinforma.*, 2002, **49**, 1–6.
21 C. Wang, R. A. Lamb and L. H. Pinto, Activation of the M2 ion channel of influenza virus: a role for the transmembrane domain histidine residue, *Biophys. J.*, 1995, **69**, 1363–1371.
22 W. W. Cleland, Low-Barrier Hydrogen Bonds and Enzymatic Catalysis, *Arch. Biochem. Biophys.*, 2000, **382**, 1–5.
23 E. F. Aziz, W. Eberhardt and S. Eisebitt, Effect of Cysteine vs. Histidine on the Electronic Structure of Zn2+ Upon Complex Formation, *Z. Für Phys. Chem.*, 2008, **222**, 727–738.
24 A. Lampel, Biology-Inspired Supramolecular Peptide Systems, *Chem*, 2020, **6**, 1222–1236.
25 A. Levin, T. A. Hakala, L. Schnaider, G. J. L. Bernardes, E. Gazit and T. P. J. Knowles, Biomimetic peptide self-assembly for functional materials, *Nat. Rev. Chem.*, 2020, **4**, 615–634.
26 W. Lu, E. Zhang, C. Amarasinghe, O. Kostko and M. Ahmed, Probing Self-Assembly in Arginine–Oleic Acid Solutions with Terahertz Spectroscopy and X-ray Scattering, *J. Phys. Chem. Lett.*, 2020, **11**, 9507–9514.
27 B. Gabryelczyk, H. Cai, X. Shi, Y. Sun, P. J. M. Swinkels, S. Salentinig, K. Pervushin and A. Miserez, Hydrogen bond guidance and aromatic stacking drive liquid-liquid phase separation of intrinsically disordered histidine-rich peptides, *Nat. Commun.*, 2019, **10**, 5465.
28 L. H. Al-Madhagi, S. K. Callear and S. L. M. Schroeder, Hydrophilic and hydrophobic interactions in concentrated aqueous imidazole solutions: a neutron diffraction and total X-ray scattering study, *Phys. Chem. Chem. Phys.*, 2020, **22**, 5105–5113.
29 B. M. Messer, C. D. Cappa, J. D. Smith, W. S. Drisdell, C. P. Schwartz, R. C. Cohen and R. J. Saykally, Local Hydration Environments of Amino Acids and Dipeptides Studied by X-ray Spectroscopy of Liquid Microjets, *J. Phys. Chem. B*, 2005, **109**, 21640–21646.
30 B. M. Messer, C. D. Cappa, J. D. Smith, K. R. Wilson, M. K. Gilles, R. C. Cohen and R. J. Saykally, pH Dependence of the Electronic Structure of Glycine, *J. Phys. Chem. B*, 2005, **109**, 5375–5382.
31 J. Gråsjö, E. Andersson, J. Forsberg, L. Duda, E. Henke, W. Pokapanich, O. Björneholm, J. Andersson, A. Pietzsch, F. Hennies and J.-E. Rubensson, Local Electronic Structure of Functional Groups in Glycine As Anion, Zwitterion, and Cation in Aqueous Solution, *J. Phys. Chem. B*, 2009, **113**, 16002–16006.
32 M. Blum, M. Odelius, L. Weinhardt, S. Pookpanratana, M. Bär, Y. Zhang, O. Fuchs, W. Yang, E. Umbach and C. Heske, Ultrafast Proton Dynamics in Aqueous Amino Acid Solutions Studied by Resonant Inelastic Soft X-ray Scattering, *J. Phys. Chem. B*, 2012, **116**, 13757–13764.
33 F. Meyer, M. Blum, A. Benkert, D. Hauschild, S. Nagarajan, R. G. Wilks, J. Andersson, W. Yang, M. Zharnikov, M. Bär, C. Heske, F. Reinert and L. Weinhardt, "Building Block Picture" of the Electronic Structure of Aqueous Cysteine Derived from Resonant Inelastic Soft X-ray Scattering, *J. Phys. Chem. B*, 2014, **118**, 13142–13150.
34 M. Faubel, B. Steiner and J. P. Toennies, Photoelectron spectroscopy of liquid water, some alcohols, and pure nonane in free micro jets, *J. Chem. Phys.*, 1997, **106**, 9013–9031.
35 D. Nolting, E. F. Aziz, N. Ottosson, M. Faubel, I. V. Hertel and B. Winter, pH-Induced Protonation of Lysine in Aqueous Solution Causes Chemical Shifts in X-ray Photoelectron Spectroscopy, *J. Am. Chem. Soc.*, 2007, **129**, 14068–14073.
36 N. Ottosson, K. J. Børve, D. Spångberg, H. Bergersen, L. J. Sæthre, M. Faubel, W. Pokapanich, G. Öhrwall, O. Björneholm and B. Winter, On the Origins of Core−Electron Chemical Shifts of Small

Biomolecules in Aqueous Solution: Insights from Photoemission and ab Initio Calculations of Glycineaq, *J. Am. Chem. Soc.*, 2011, **133**, 3120–3130.
37 D. Nolting, N. Ottosson, M. Faubel, I. V. Hertel and B. Winter, Pseudoequivalent Nitrogen Atoms in Aqueous Imidazole Distinguished by Chemical Shifts in Photoelectron Spectroscopy, *J. Am. Chem. Soc.*, 2008, **130**, 8150–8151.
38 B. Xu, M. I. Jacobs, O. Kostko and M. Ahmed, Guanidinium Group Remains Protonated in a Strongly Basic Arginine Solution, *ChemPhysChem*, 2017, **18**, 1503–1506.
39 A. Barrozo, B. Xu, A. O. Gunina, M. I. Jacobs, K. Wilson, O. Kostko, M. Ahmed and A. I. Krylov, To Be or Not To Be a Molecular Ion: The Role of the Solvent in Photoionization of Arginine, *J. Phys. Chem. Lett.*, 2019, **10**, 1860–1865.
40 J. G. Mesu, T. Visser, F. Soulimani and B. M. Weckhuysen, Infrared and Raman spectroscopic study of pH-induced structural changes of l-histidine in aqueous environment, *Vib. Spectrosc.*, 2005, **39**, 114–125.
41 V. Feyer, O. Plekan, N. Tsud, V. Cháb, V. Matolín and K. C. Prince, Adsorption of Histidine and Histidine-Containing Peptides on Au(111), *Langmuir*, 2010, **26**, 8606–8613.
42 V. Feyer, O. Plekan, S. Ptasińska, M. Iakhnenko, N. Tsud and K. C. Prince, Adsorption of Histidine and a Histidine Tripeptide on Au(111) and Au(110) from Acidic Solution, *J. Phys. Chem. C*, 2012, **116**, 22960–22966.
43 Y. Zubavichus, A. Shaporenko, M. Grunze and M. Zharnikov, Innershell Absorption Spectroscopy of Amino Acids at All Relevant Absorption Edges, *J. Phys. Chem. A*, 2005, **109**, 6998–7000.
44 V. Carravetta, O. Plashkevych and H. Ågren, A theoretical study of the near-edge x-ray absorption spectra of some larger amino acids, *J. Chem. Phys.*, 1998, **109**, 1456–1464.
45 S. Eckert, J. Niskanen, R. M. Jay, P. S. Miedema, M. Fondell, B. Kennedy, W. Quevedo, M. Iannuzzi and A. Föhlisch, Valence orbitals and local bond dynamics around N atoms of histidine under X-ray irradiation, *Phys. Chem. Chem. Phys.*, 2017, **19**, 32091–32098.
46 O. Kostko, B. Xu, M. I. Jacobs and M. Ahmed, Soft X-ray spectroscopy of nanoparticles by velocity map imaging, *J. Chem. Phys.*, 2017, **147**, 013931.
47 G. A. Garcia, L. Nahon and I. Powis, Two-dimensional charged particle image inversion using a polar basis function expansion, *Rev. Sci. Instrum.*, 2004, **75**, 4989–4996.
48 M. J. Frisch, G. W. Trucks, H. B. Schlegel, G. E. Scuseria, M. A. Robb, J. R. Cheeseman, G. Scalmani, V. Barone, B. Mennucci, G. A. Petersson, H. Nakatsuji, M. Caricato, X. Li, H. P. Hratchian, A. F. Izmaylov, J. Bloino, G. Zheng, J. L. Sonnenberg, M. Hada, M. Ehara, K. Toyota, R. Fukuda, J. Hasegawa, M. Ishida, T. Nakajima, Y. Honda, O. Kitao, H. Nakai, T. Vreven, J. A. Montgomery Jr., J. E. Peralta, F. Ogliaro, M. J. Bearpark, J. Heyd, E. N. Brothers, K. N. Kudin, V. N. Staroverov, R. Kobayashi, J. Normand, K. Raghavachari, A. P. Rendell, J. C. Burant, S. S. Iyengar, J. Tomasi, M. Cossi, N. Rega, N. J. Millam, M. Klene, J. E. Knox, J. B. Cross, V. Bakken, C. Adamo, J. Jaramillo, R. Gomperts, R. E. Stratmann, O. Yazyev, A. J. Austin, R. Cammi, C. Pomelli, J. W. Ochterski, R. L. Martin, K. Morokuma, V. G. Zakrzewski, G. A. Voth, P. Salvador, J. J. Dannenberg, S. Dapprich, A. D. Daniels, Ã. Farkas, J. B. Foresman, J. V. Ortiz, J. Cioslowski and D. J. Fox, *Gaussian 09*, Gaussian, Inc., Wallingford, CT, USA, 2009.
49 S. Tardio and P. J. Cumpson, Practical estimation of XPS binding energies using widely available quantum chemistry software, *Surf. Interface Anal.*, 2018, **50**, 5–12.
50 A. Sadybekov and A. I. Krylov, Coupled-cluster based approach for core-level states in condensed phase: Theory and application to different protonated forms of aqueous glycine, *J. Chem. Phys.*, 2017, **147**, 014107.
51 J. M. Pi, M. Stella, N. K. Fernando, A. Y. Lam, A. Regoutz and L. E. Ratcliff, Predicting Core Level Photoelectron Spectra of Amino Acids Using Density Functional Theory, *J. Phys. Chem. Lett.*, 2020, **11**, 2256–2262.

339

Table 1: Summary of all experimental C1s and N1s binding energies (in eV) for histidine aqueous aerosol generated at different pH conditions.

	C1s				N1s		
	carboxyl	amine, N=C–NH	C–N	C–C	amine	N=C–NH	N=C–NH
pH = 1	293.3	291.6	290.9	290.6	406.6	406.0	405.6
pH = 7	292.5	290.8	290.0	289.8	406.1	405.0	403.6
pH = 13	292.3	290.5	290.0	289.3	403.9	405.0	403.2

Table 2: Summary of all calculated C1s and N1s binding energies (in eV) for histidine aqueous aerosol generated at different pH conditions.

	C1s						N1s		
	carboxyl	amine	N=C–NH	C–NH	C–N	C–C	amine	N=C–NH	N=C–NH
pH = 1	294.4	292.4	292.5	291.2	291.5	290.8	407.5	406.3	406.3
pH = 7	292.2	290.9	290.9	290.0	290.0	289.8	405.9	405.1	403.6
pH = 13	291.7	289.8	290.8	289.9	289.8	289.2	402.8	405.0	403.5

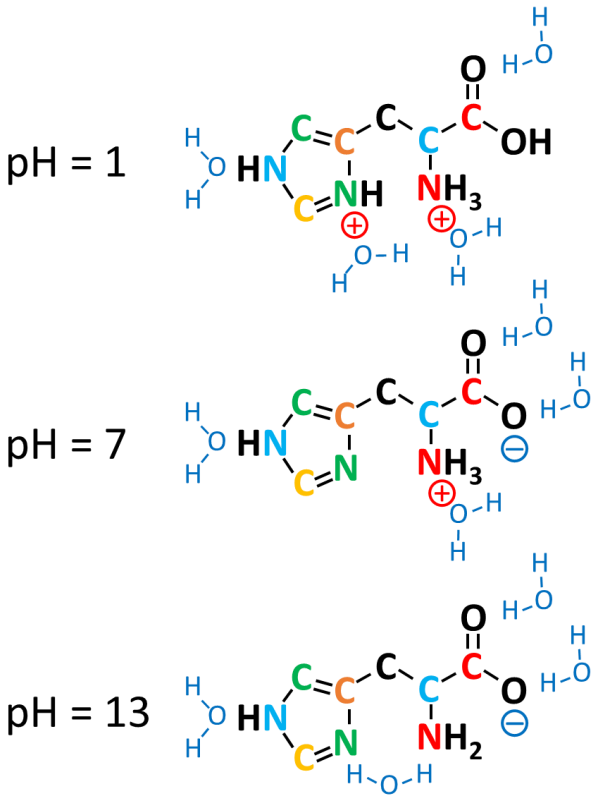

347

348 Figure 1. Dominating protonation forms of histidine in aqueous solution at different pH conditions.

349

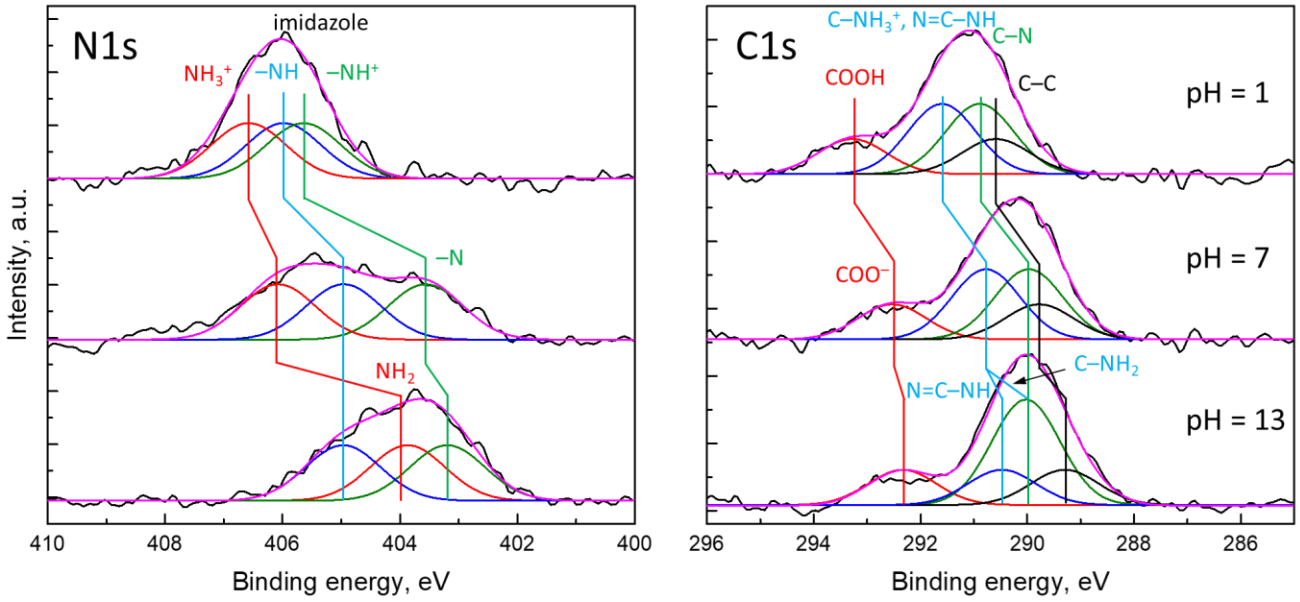

Figure 2. N1s and C1s photoelectron spectra of aqueous histidine collected at pH = 1 (top), pH = 7 (middle), and pH = 13 (bottom). Black line represents experimental data, while magenta line represents total fit composed of sum of individual Gaussians (colored in red, blue, green, and black).

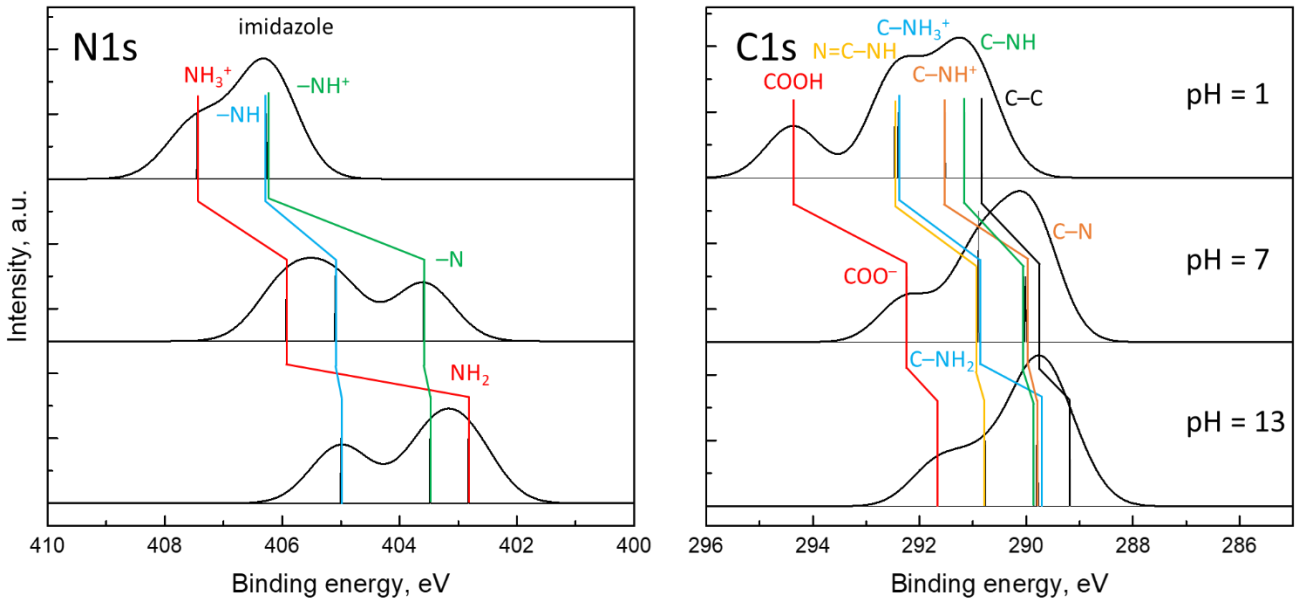

Figure 3. Theoretical N1s and C1s spectra of aqueous histidine collected at pH = 1 (top), pH = 7 (middle), and pH = 13 (bottom). Calculated binding energies are shown with vertical colored sticks. The spectrum is convoluted with Gaussian (FWHM = 1.2 eV) to correlate with the experimental photoelectron spectra and shown as black lines.